Journal of Materials Research and Technology 28 (2024) 1062–1073

Contents lists available at ScienceDirect

Journal of Materials Research and Technology

journal homepage: www.elsevier.com/locate/jmrt

Optimising a processing window for the production of aluminium silicon-12 samples via selective laser melting

Alliance Gracia Bibili Nzengue [a,*], Khumbulani Mpofu [a], Ntombizodwa Ruth Mathe [b], Rumbidzai Muvunzi [c]

[a] Department of Industrial Engineering, Tshwane University of Technology, Staartsartillirie Road, Pretoria West, Pretoria, 0183, South Africa
[b] Laser Enabled Manufacturing, Photonics Centre, Council for Scientific and Industrial Research, Meiring Naudé Road Brummeria, Pretoria, 0001, South Africa
[c] Department of Industrial and Systems Engineering, Cape Peninsula University of Technology, Bellville South Industrial, Cape Town, 7535, South Africa

ARTICLE INFO

Handling Editor: L Murr

Keywords:
AlSi12
Selective laser melting
Response surface methodology
Physical properties
Mechanical properties

ABSTRACT

Selective laser melting (SLM) SLM has gained interest in processing lightweight metals like aluminium alloys. The SLM processing remains challenging in finding the appropriate process parameters for the desired mechanical properties. Previous studies have used energy density formulas and heat treatment to improve the mechanical properties of materials in different ways. However, the holistic approach to studying the physical and mechanical properties has less been reported. Therefore, this article presents the optimisation of the processing window of the AlSi12 aluminium alloy produced by the SLM process. The design of the experiment (DoE) was carried out using the Response Surface Methodology (RSM) implemented in the Design Expert 2018 environment. It involved two process factors in the following range of scan speed (500–2500 mm/s) and laser power (50–300 W). The combination of a scan speed of 500 mm/s and a laser power of 300 W resulted in a relative density of 97.4 %, an ultimate tensile strength (UTS) of 418 MPa and a hardness of 132.6 HV. The microstructure and fracture analysis provided evidence of reduced defects with the combination of parameters mentioned above. Thus, this study contributes to adding a new set of data to existing work for more comprehensive parameter calibration. This study helps industries that produce aluminium alloys from SLM processes obtain the optimal range of process parameters that produce parts with the desired mechanical properties.

1. Introduction

Aluminium-silicon alloys have gained increasing application in the automotive and aerospace industries due to their excellent corrosion resistance, low ductility, formability, high strength-to-weight ratio, and low density [1]. The low-density property of Al alloys makes them critical in applications where lightweight material is required. This has contributed to their widespread use in the transport sector, where it is necessary to reduce fuel and energy consumption, and consequently the carbon footprint [2].

AlSi10Mg and AlSi12 alloys are casting alloys that have been extensively reported using conventional manufacturing methods. However, processing these alloys with conventional methods results in undesirable mechanical properties such as cracks and porosity for applications, for example, aerospace [3]. Therefore, research on processing methods continues to achieve improved mechanical properties [4]. One of the processing techniques that has provided an opportunity to achieve mechanical properties that meet the application requirements is additive manufacturing (AM) processes, specifically the selective laser melting process [5].

Selective laser melting (SLM) is a process that belongs to powder bed fusion (PBF) for the production of metal parts [1]. It is known for its ability to produce highly complex geometries and its vast scalability [3]. It has revealed great potential for producing nearly fully dense and almost net-shaped parts that produce improved mechanical properties compared to conventional processing methods [6]. The SLM process encompasses many laser- and scan-related parameters that influence the melting pool. These process-related parameters must be controlled to ensure defect-free parts [4].

Despite efforts to optimise the processing window to achieve fully dense parts, defects are still observed within SLM-manufactured Al alloy parts that require further investigation [7]. These defects are due to

* Corresponding author.
E-mail addresses: alliancebibili@gmail.com, 213090062@tut4life.ac.za (A.G. Bibili Nzengue), MpofuK@tut.ac.za (K. Mpofu), NMathe@csir.co.za (N.R. Mathe), Muvunzir@cput.ac.za (R. Muvunzi).

https://doi.org/10.1016/j.jmrt.2023.11.233
Received 19 September 2023; Received in revised form 25 November 2023; Accepted 25 November 2023
Available online 7 December 2023

rapid cooling and heating rates, which are generally higher than the conventional welding process [4]. Furthermore, the repetitive cooling and heating process, which is guided by the AM principle of layer-by-layer deposition of powder to create a part, can potentially cause unmelted powder, lack of fusion, residual stress, and porosity [4,7]. All of these are potential factors that decrease the strength of the material and initiate fatigue cracks [7].

The variability in the mechanical behaviour obtained is due to the lack of standardisation of the processing parameters for Al alloys, which is observed by measurements of fatigue resistance and tensile strength [8]. The lack of standardisation emanates from the challenging interplay of the laser, scan, powder, and temperature-related parameters. Prashanth and Scudino [9] used a laser power of 320 W and scanning speeds of 1455 mm/s and 1939 mm/s for the volume and contour of the Al–12Si samples on an SLM 250 HL equipment to define the tensile properties. Other parameters included a layer thickness of 50 μm, a 73° hatch rotation with a hatch spacing of 110 μm, temperatures of 473 K, 573 K, and 673 K for base plate heating, followed by an ex-situ heat treatment ranging between 473 K and 723 K for 6 h. Their findings indicated that variations in hatch style resulted in an improved ultimate tensile strength (UTS) of approximately 460 MPa compared to samples produced with base plate heating. A comparison of the in-situ variation and ex-situ variation revealed that the tensile behaviour is related to crack propagation. Although the ductility of the material was improved by reducing the cooling rates, the UTS was lower than that of the other strategies. Heat treatment, as reported by the authors, is responsible for the decrease in the material strength.

Furthermore, Aboulkhair et al. [7] looked at the nanoscale, microscale, and macroscopic scales to determine the effect of conventional heat treatment on mechanical properties. A laser power of 200 W, hatch spacing of 130 μm, scanning speed of 80 μm, and a layer thickness of 25 μm, were used to produce the samples.

Several critical parameters [10–12] have been reported to optimise the quality of the part in situ. Some parametric studies have been conducted to determine the impact of an inadequate combination of parameters on the formation of defects [13–15]. Buchbinder et al. [16], recommended up to 1 kW laser power due to the high reflectivity of Al alloys. They proposed an interaction time ranging from 4×10^{-3} to 4×10^{-4} s, a layer thickness of 50 μm and a scanning rate of 1700 mm/s to achieve close to 100 % densities. The authors revealed that the laser power used to melt the powder plays a critical role in the number of resulting defects, which decreases the density. The experiment resulted in a tensile strength of 400 MPa with a density of 99.5 %. Whereas Fefelov et al. [10] and Zhuo et al. [17] used relatively lower scanning speeds and laser powers, they obtained UTS of 446 MPa for AlSi10Mg and 425 MPa for AlSi12.

Among the process-related parameters, laser power, hatching space, layer thickness, scanning speed, and scanning strategy have received much attention [3,4]. These studies revealed that the stability of the melt pool is determined by the amount of energy required to fill a scan track. Therefore, previous studies [18,19] have based the improvement of mechanical and microstructural properties on the energy density (E, J/mm^3) using Eq. (1) below:

$$E = \frac{p}{V\,h\,t} \tag{1}$$

Here, p is the laser power (W), V is the scan speed (mm/s), h is the hatch spacing (mm) and t is the layer thickness (mm). According to Prashanth et al. [20] Eq. (1) needs modification as it does not always ensure the required results. With different parameters (p and v), the same value of E can be obtained [21].

The shortcoming observed in improving the mechanical properties of Al alloys with heat treatment and the energy density formula has attracted attention to the design of experiments (DOE) and statistical approaches. In a related development, Mathe [22] used the response surface methodology (RSM) and proposed a 1400 W laser power processing window with a laser interaction time of $1.63–1.95 \times 10^{-4}$s, and the authors obtained a UTS of 310 MPa for AlSi10Mg samples. It should be noted that the laser power of the Council for Scientific and Industrial Research (CSIR) machine built in house used in their research was higher than that of many of the commercially available SLM machines. Similarly, Terner et al. [23] proposed RSM as a reliable approach to determine the influence of process parameters (scanning speed, laser power, scanning strategy, layer thickness, and hatch spacing) on the hardness, microstructure, and density of the CoCr–Mo alloy. Bai et al. [11] used RSM to investigate the effect of varying the laser power, hatch spacing, and scan speed on the microstructure, relative density, and microhardness of the AlSiMg0.75 alloy, as built and annealed samples. Other scholars have also explored this methodology with four factors to define the microstructure, tensile properties, and microhardness of AlSi10Mg alloys [23–25]. Establishing the optimal range of process parameters that will produce parts with the desired mechanical properties of the AlSi12 SLM of AlSi12 is still under investigation and has not been widely reported.

Despite the findings that laser power and scan speed have a higher influence on the properties of the SLM-produced parts; few studies have addressed the optimisation of these parameters to achieve a holistic improvement of physical and mechanical properties than conventional processing methods. The work carried out was experimental and theoretical. The development of a predictive model equation using design Expert RSM for determining the magnitude of the density, hardness, and UTS as a function of the process parameters, namely scan speed and laser power, has not been sufficiently highlighted by the existing literature. Thus, this article contributes to the development of a process parameter window and determines the interaction of the parameters with the densification, microstructure and mechanical properties of AlSi12, through the development of a predictive model. The results of this work will guide the industry in choosing the SLM building parameters for the desired application.

2. Materials and methods

2.1. Material

The AlSi12 powder was supplied by TLS Technik GmbH, with a particle size of 13–63 μm. The core elements in the powder are Al (88.97 %) and Si (11.8 %). The powder was processed as purchased.

2.2. Processing

The commercial SLM Solution M280, equipped with a 400 W laser and a beam focus diameter of 80–115 μm was used to fabricate the samples in a closed loop system; with an inert argon gas that prevents oxidation and collects impurities [26]. The cylindrical specimens were built in a vertical direction with a diameter of 10 mm and a length of 80 mm. All samples were fabricated using a constant layer thickness of 30 μm and a hatch distance of 0.5 mm.

2.3. Experimental design

The design of the experiments followed two sets of trial runs. During the first stage, the response surface method (RSM) is used (1) to design the building matrix and (2) to determine the optimal range of parameters. This process also helps to predict the importance of different factors, such as laser power (W) and scanning speed (mm/s). The second set of experiments is formulated to hypothetically test that laser power greatly affects the structural integrity of the fabricated samples.

Response Surface Methodology (RSM) was implemented in the Design Expert 2018 software. RSM helps solve engineering problems by studying the effect of independent variables (factors) on dependent variables (responses) for process optimisation [27]. The identified factors are laser power (50–300 W) and scanning speed (500–2500 mm/s).

The range of factors selected in this study is discussed in the previous study [28]. The model entails a two-level factorial design; hence, consideration is made for the central composite design (CCD). The CCD model is expressed as 2^k factorials (with k as the factor number) [29]. The two levels of the factorial trials are coded from −1 to +1. The number of experiments was randomly generated, based on the orthogonality and rotatability of the CCD model. The number of runs (N) is determined using Eq. (2) [27].

$$N = 2^k + 2K + n_0 \tag{2}$$

Where n_0 is the number of centre points and k is the number of factors.

Table 1 presents the coded levels of the factors using Eq. (2).

The most commonly used mathematical model to fit experimental data is the polynomial quadratic equation. The equation describes the interaction of the factors expressed in Eq. (3) [27,29].

$$Y = \beta_o + \sum_{i=1}^{k} \beta_i X_i + \sum_{i=1}^{k} \beta_{ii} X_i^2 + \sum_{j} \sum_{<i=1}^{k} \beta_{ij} X_i X_j + \varepsilon \tag{3}$$

Y depicts the predicted response; β_o is a constant; X_i *and* X_j are the varied factors; β_j,β_{ij} *and* β_{jj} are respectively the linear coefficients, second order and quadratic coefficients, and ε is the experimental random error. In this study, the factors were coded as A (Laser power) and B (scanning speed); hence the equation can be written as:

$$Y = \beta_o + \beta_i A + \beta_i B + \beta_{ii} A^2 + \beta_{ii} B^2 + \beta_{ij} AB \tag{4}$$

The results of the model were computed in the design expert software and analysed by applying analysis of variance (ANOVA). In the approach, the model is significant at 95 % on the assumption that the mean square P value < 0.05 [21]. Another statistical expression used to verify the model is the R^2 values, which express the prediction compatibility of the model. The R^2, correlation coefficient includes $R^2_{adjusted}$ and $R^2_{predicted}$. R^2 and $R^2_{adjusted}$ values should be near or close to 1, while the value of $R^2_{adjusted} - R^2_{predicted}$ should be less than 0.2 [27].

2.4. Testing procedure of the samples

The mechanical test involved performing a tensile test using Instron 1342 (ASTM A370) to analyse and measure the properties of the materials, such as the strength of performance, the maximum strength of the tensile, the modulus of elasticity, and elongation. The test was carried out with the following characteristics: a test speed of 0.5 mm/min; load capacity of 25 kN; extensometer gauge length of 27.5 mm; a travel length of 5 mm; and a specimen gauge length marked 30 mm to obtain the percentage of elongation. The samples were in the dog bone shape as presented in Fig. 1 (a). JEOL JSM scanning electron microscope (SEM) was used to analyse the fracture point after the tensile test. The density of the as-built samples was measured using the Archimedes technique with the Ohaus densitometer. To determine the densification and structure of the samples, the microstructure was observed using an Olympus BX51 M optical microscope on polished and etched samples with Keller's agent, as indicated in Fig. 1(b). The hardness was measured using a Zwick Micro/Macro HV hardness (ASTM E92) with a force of 300 gf and a dwell time of 10 s. Measurements were made in both cross-sectional samples in Fig. 1(b). Recorded averages were used for analysis.

3. Results and discussion

3.1. Powder analysis

The composition of the investigated AlSi12 alloy is shown in Table 2. The particle morphology was close to spherical, which influences the flowability of the powder during the SLM process.

Fig. 2 (a) presents the powder scanning electron microscope (SEM) micrograph [13], Fig. 2 (b) the SEM electrostatic discharge spectrum (ESD), and Fig. 2(c) shows the distribution of the Al and Si content.

3.2. Density, hardness, and ultimate tensile strength measurements

The DOE for the first batch provided a combination of 14 runs. However, after the SLM fabrication process, only six samples (S2, S3, S7, S11, S12 and S14) were considered for further analysis. This was due to the high amount of porosity that prevented the samples from being machined. A detailed explanation is found in a previous study [28]. Table 3 presents the randomised design matrix for the experimental runs with the measured response values. The study focused on data on the ultimate tensile strength (UTS) due to its ability to determine the strength of the material for the desired application [12].

The second set of experiments is based on the observations made on the results obtained in Table 3. The scan speed is kept constant at 500 mm/s, and the laser power (W) values were narrowed to identify the optimal combination of parameters. The laser power was varied from 175 W to 300 W as presented in Table 4. The design of the experiment followed an optimal design with one numeric factor to determine the effect of the laser power on the physical and mechanical properties of the AlSi12 SLM-fabricated samples.

3.3. Microstructure analysis

The microstructure observed in Fig. 3 exhibits the reported "fish scale" structure [30]. However, the presence of unmelted powder is visible on samples that were built at a scan speed above 500 mm/s. The larger cooling and solidification cycles-initiated dislocation in the samples that affected the melting pool. The heat transmission did not follow an even pattern, leading to partially melted layers, as depicted by the S3, S7, S11, and S14 microstructures. The variation of the molten pool can also be attributed to the scan speed values, which are higher compared to the laser power. This means that the energy was insufficient to create a solidification of the powder when melting the previous layer.

At 500 mm/s the microstructures of S2 (300 W) and S12 (175 W), have a small number of pores and reduced traces of unmelted powder. This delivered an integral physical structure. The pores observed on S2 are spherical from the trapped gas, while on the other specimens; the pores are located at the boundaries of the molten pool. The last pores are irregular and are mainly due to unmelted powder [31]. The inhomogeneities and grain size on the samples are the result of the distortion in the thermal gradients caused by the combination of laser power and scan speed. This corroborates that the level of porosity and growth of the grain size can be controlled by the processing window [13–15].

After the microstructure of the first batch, the processing window was narrowed [175 W–300 W] and varied at 25 W intervals, to improve the densification of the samples. The scan speed was kept constant at 500 mm/s because the consolidation occurred at that speed in the first experiment. Fig. 4 shows the improvement in the microstructure of the

Table 1
Experimental design matrix for process parameters.

Factors	Name	Units	Low	High	Low coded	High coded	Mean	Std. Dev.
A	Laser Power	W	50.00	300.00	−1.000	1.000	180.357	84.610
B	Scanning Speed	mm/s	500.00	2500.00	−1.000	1.000	1375.000	646.073

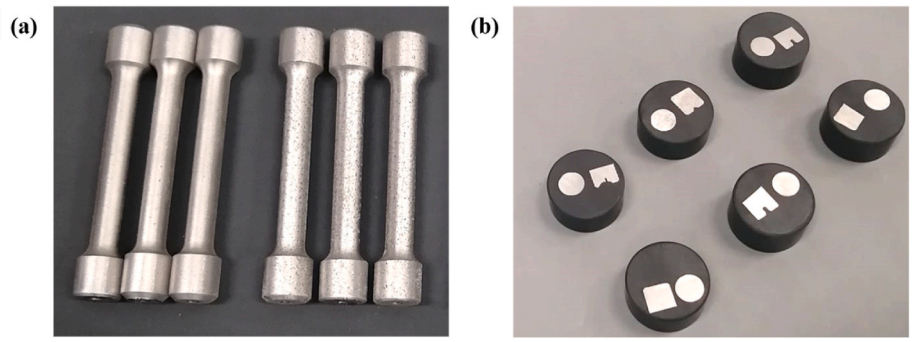

Fig. 1. Tensile specimens; (b) cross-sectional mounted specimens.

Table 2
Chemical composition of AlSi12 (Wt%).

Al	Mg	Si	Ca	Fe	K	Na
88.97	<0.01	11.8	0.05	0.17	0.03	0.07

fabricated samples.

The micrographs of C, D and E have fewer pores compared to those of A, B and F. The decrease in scan speed promotes the lower level of porosity observed in the samples. This confirms that the heat input increases as the laser power increases; this makes the molten pool larger and facilitates the consolidation of a larger amount of powder [31]. It is evident that the different melt pools are intercepted by fine dendritic structures with columnar grains. High cooling rates promote the evolution of finer cellular dendritic structures. The mechanism of cellular dendritic structures is complex and is not apparent on micrographs. The grain structures were equiaxed for D and F. Several studies have reported the formation of grain structures of AlSi12 and the non-equilibrium phases of the Al and Si content in the microstructure [4, 32–34].

3.4. Mechanical properties of AlSi12 samples analysis

Variations in UTS and hardness were recorded with different combinations of parameter values (Tables 3 and 4). The high porosity that affected the results of S3, S7, S11, and S14 led to UTS values ranging from 71 MPa to 148 MPa and hardness ranging from 66.8 HV to 133.3 HV. Although the cast counterpart AlSi12 UTS is approximately 170–205 MPa [35], the results obtained revealed that the processing window is limited and may not be considered for further research. The findings indicate that an increase in the scan speed results in a reduction of the UTS and the hardness of AlSi12 fabricated through SLM. While an increase in laser power might guarantee sufficient energy input to melt

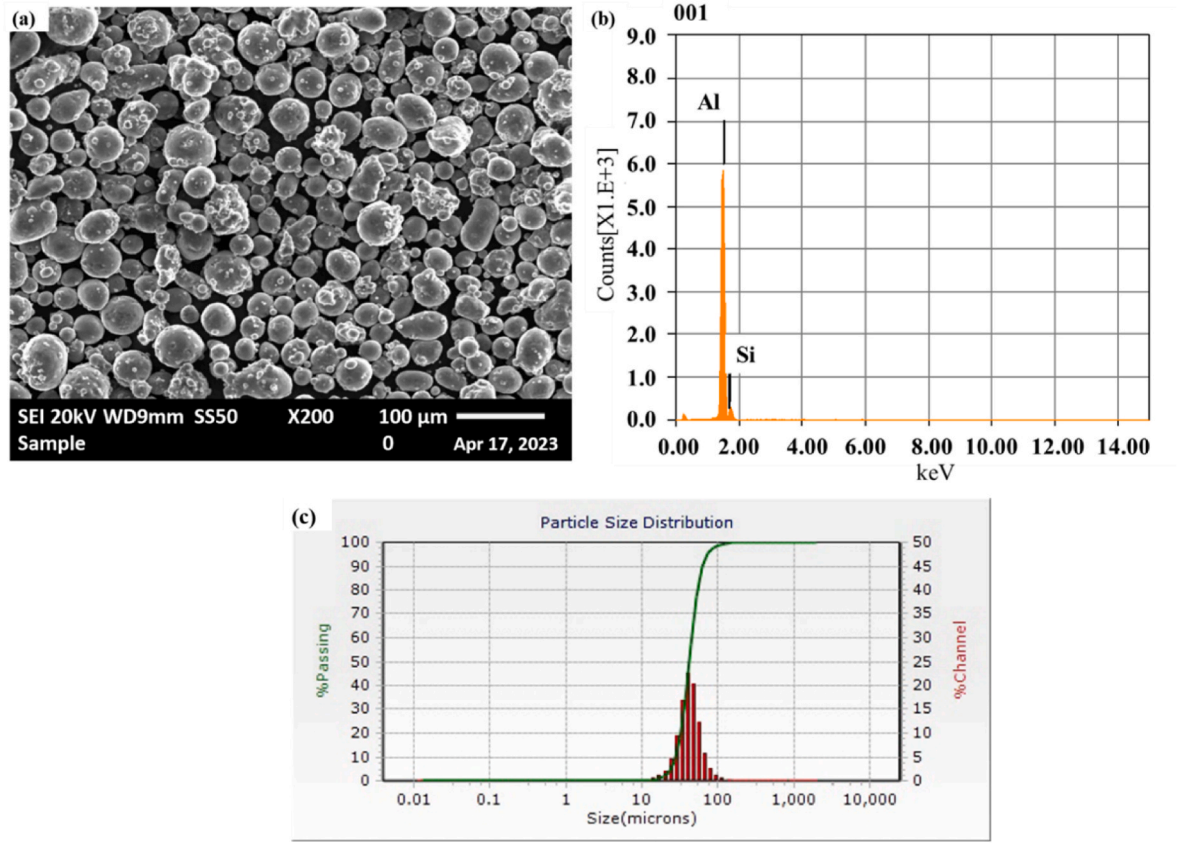

Fig. 2. (a) Morphology of AlSi12 from SEM; (b) SEM EDS spectrum from SEM; (c) Powder distribution (from supplier).

Table 3
Building matrix parameters (batch 1).

Runs [S]	Factors		Responses		
	Laser power (W)[A]	Scanning speed (mm/s)[B]	Relative Density(%)	Hardness (HV)	Ultimate Tensile Strength (MPa)
1	175	1500	–	–	–
2	300	500	95.14	133.3	418.42
3	300	2500	87.44	77.9	71.67
4	50	500	–	–	–
5	50	2500	–	–	–
6	175	2000	–	–	–
7	175	1000	87.73	81.4	76.09
8	175	750	–	–	–
9	50	1500	–	–	–
10	150	1500	–	–	–
11	300	1500	90.08	101.8	148.38
12	175	500	93.19	132.6	256.93
13	200	1500	–	–	–
14	250	1500	86.51	82.7	79.72

Table 4
Design matrix batch 2.

Runs	Factors	Response values		
	Laser Power (W)	Relative Density (%)	Hardness [HV]	Ultimate Tensile Strength(MPa)
A	175	93.03	70.8	231.76
B	200	95.8	66.8	329.29
C	225	97.2	70.5	378.83
D	250	97.4	75.2	398.25
F	275	96.3	118.6	403.25
E	300	97.4	116.6	415.58

the deposited powder particles. This was observed in the first experiment, as the highest UTS of S2 (300 W) was 418 MPa; while in the second experiment, it was 415 MPa. The slight difference can be attributed to the flowability of the powder, which was recycled. Furthermore, the results of this study corroborate with previous studies (Table 4) since the value of S2 exceeded some of the results in Table 5 for hardness and UTS. The machine used has been reported to have an impact on the fabricated SLM parts [16]. This is evidenced in the previous study where the laser power was set at 200 W and the scan speed was set at 375–2000 mm/s [12]. For comparison, the maximum UTS achieved was 368 MPa, which is less than 418 MPa in this study.

3.5. Analysis of fracture morphology

The fracture behaviour of AlSi12 for the two stages of the experiments ensures that a significant measure of ductility was observed, as indicated in Figs. 5 and 6. Round dimples can be observed in Figs. (5 and 6) for S2, S12 D, E and F that occur as plastic deformation at the rupture point. For samples 3 and 14, intergranular structures and cracks were observed with the appearance of the materials. This may be due to the insufficient energy to separate the grains along the grain boundaries. This leads to the appearance of secondary cracks that propagate on the surfaces of samples 3 and 11 and culminate in several fracture cleavage steps in the fracture morphology. There is evidence of improperly melted powder particles approximately the same size as the initial powder particles on the surface of the deposited layers in samples 3, 7 and 14. Samples S11, A, B, C, and D show evidence of small dimples and minimal crack propagation on the surface compared to other samples. In the cross-sections of the samples, micropores are seen to be distributed. This may be the result of small plastic deformations restrained around the particles. The presence of cracks on the surface can also be attributed to the development of residual or internal stresses. The high-temperature gradient and the rapid cooling step can cause non-uniform

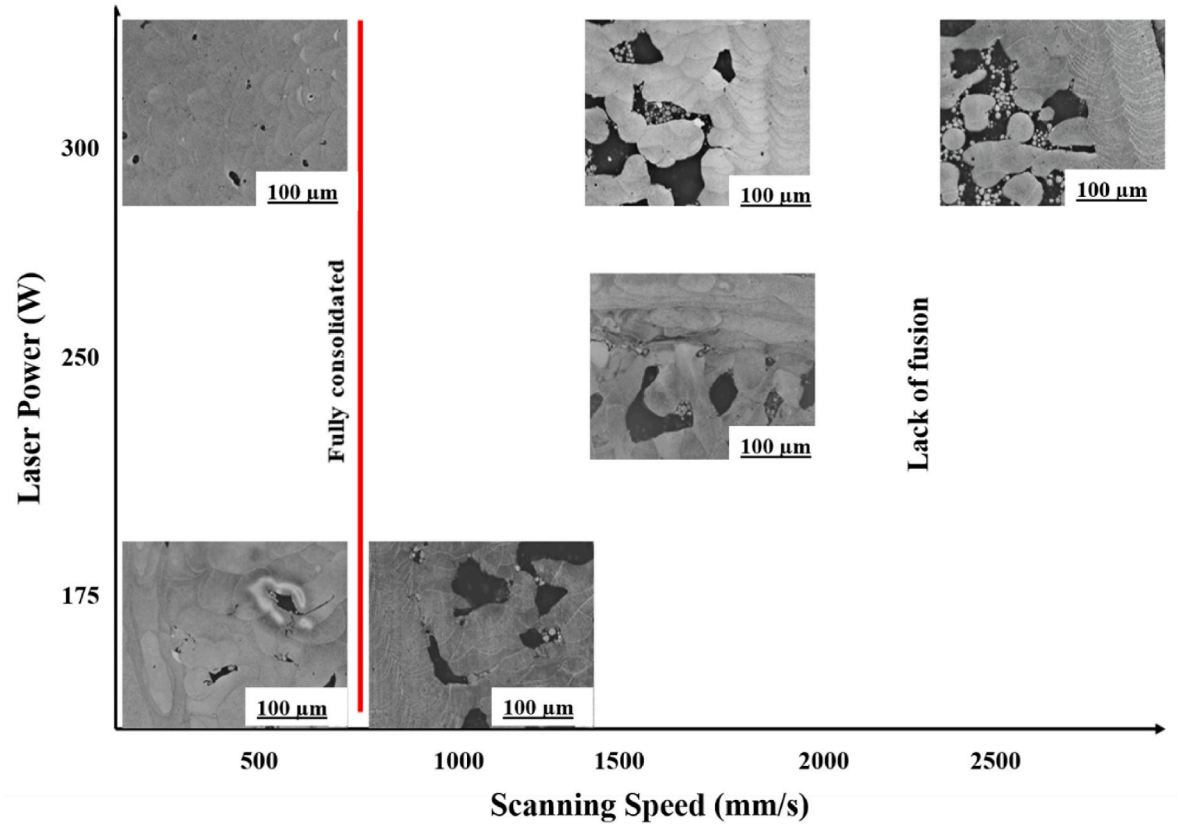

Fig. 3. Optical micrographs of the samples at different scan speeds and laser power.

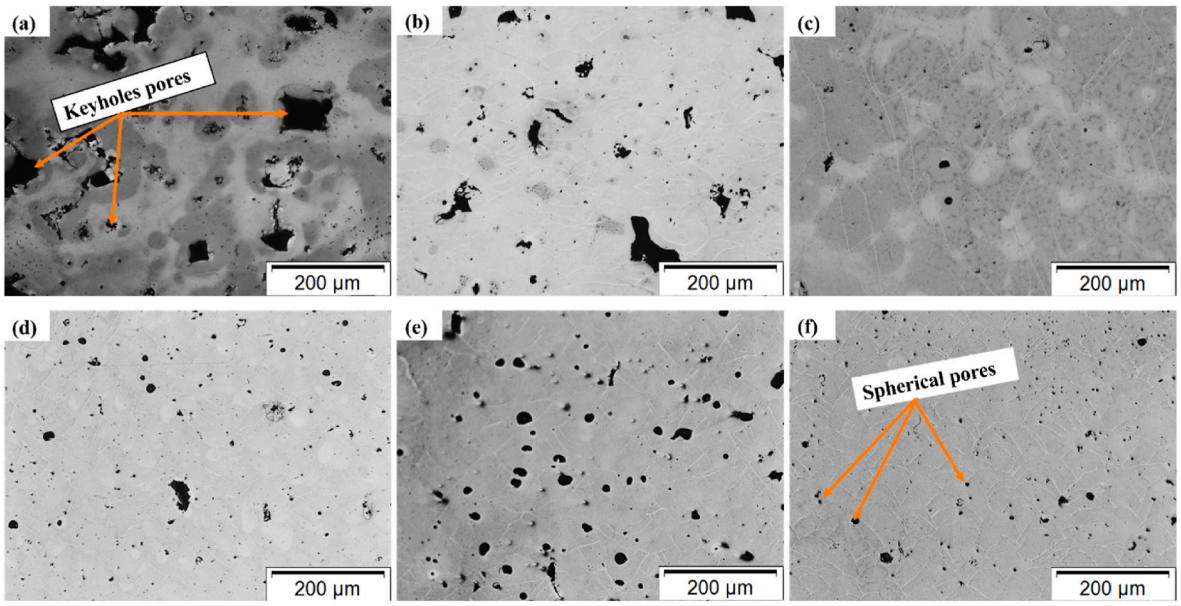

Fig. 4. Batch 2 microstructures at different laser power (W)–(a) 175 W; (b) 200 W; (c) 225 W; (d) 250 W; (e) 275 W; (f) 300 W- Lack of fusion hole observed (a, b, e); Spherical porosity (c, d, f).

Table 5
SLM of AlSi12 ultimate tensile strength and hardness comparison.

Source	Laser power (W)	Scanning speed (mm/s)	Hardness (HV)	UTS (MPa)	Machine
Current study	50–300	500–2500	66.8–133.3	71–418	
Gokuldoss et al. [12]	320	1455		385 ± 4	SLM 250 HL
Kang et al. [8]	400	5000		–	Realizer SLM 250
Ponnusamy et al. [37]	285	1000	150–160	–	3D Systems ProX 200
Prashanth et al. [9]	320	1455–1939		220–460	SLM 250 HL
Rashid et al. [33]	285	1000–2000	110 ± 10	260–365	ProX 200
Rathod et al. [36]	320	1455	73–123	–	SLM 280 HL
Wang, Zhang [34]	200	375–2000	65–115	368	Realizer SLM 100
Suryawanshi et al. [38]	320	1455–1939		325	SLM 250 HL
Siddique et al. [39]	350	930		361	SLM 250 HL

deformation, resulting in the development of residual stresses [5].

4. Proposed model using statistical analysis for optimisation

Statistical analysis was performed using analysis of variance (ANOVA) for the prediction of the output values for the first batch.

Table 6, Table 7 and Table 8 show the different summaries of the ANOVA for the responses including the source of variance, the sum of squares, the degree of freedom (df), the mean square, the F-value and the P-value.

The relative density (Table 6) F-value of 1778.55 means that the interaction of the laser power and the scan speed has a significant effect on the relative density, hardness, and UTS. There is only a 0.01 % chance that an F value this large could occur due to noise. The R^2 of 0.9983 shows a corroboration between the experimental values and the predicted results. The precision of the Adeq, which determines the signal-to-noise ratio, indicates an adequate signal at a ratio of 98.3023. The coded mathematical model derived from the software for the predictive equation can be expressed as Eq. (5):

$$\text{Relative density} = +81.97 + 7.97A - 11.27B + 6.07AB \quad (5)$$

where: A is the laser power (W) and B is the scan speed (mm/sec) as indicated in the second column of Table 5.

Eq. (5) is derived from Eq. (4) in coded form. The expected response is defined as the coded coefficients +81.97 when the laser power (A) and the scanning speed (B) are at their centre point and their coded values are at zero. The value of the predicted responses reduces to the constant. The remaining coded coefficients represent adjustments made around the average, based on the factor settings.

Table 7 presents the hardness and the 2FI model that was carried out. The value of R^2 (0.9790), and the adjusted R^2 (0.9720) were found to agree with the predicted value of R^2 (0.9593). Both values are close to 1. The Model F-value of 139.96 demonstrates that the model is significant. There is only a 0.01 % chance that an F value this large could occur due to noise. The effect of the scan speed as well as the laser power on the hardness is apparent. The mathematical model in coded factors provided by the software is expressed as Eq. (6):

$$\text{Hardness} = +31.57 + 74.19A - 99.70B + 72.17AB \quad (6)$$

The UTS model in Table 8, presents an F –F-value of 408.30 which is lower than the relative density. However, the value is still statistically significant since there is a 0.01 % chance that an F-value this large could occur due to noise. The corresponding coded equation is written as Eq. (7):

$$\text{Ultimate tensile strength} = -89.07 + 249.07A - 342.13B + 83.71AB \quad (7)$$

The "P-values" of the developed models are less than 0.0500. This shows that the 2FI models used for the responses are statistically significant. This led to confirmation that laser power and scan speed are significant terms in the optimisation of the processing window for the AlSi12 fabricated via SLM. Increasing or decreasing factors will have a significant effect on relative density, hardness, and UTS. This is consistent with the experimental results presented for the microstructure and fracture results in Figs. 3 and 5.

The regression approach was used to fit Eq. (3) to identify the significant model terms. The resultant ANOVA 2FI models are confirmed by

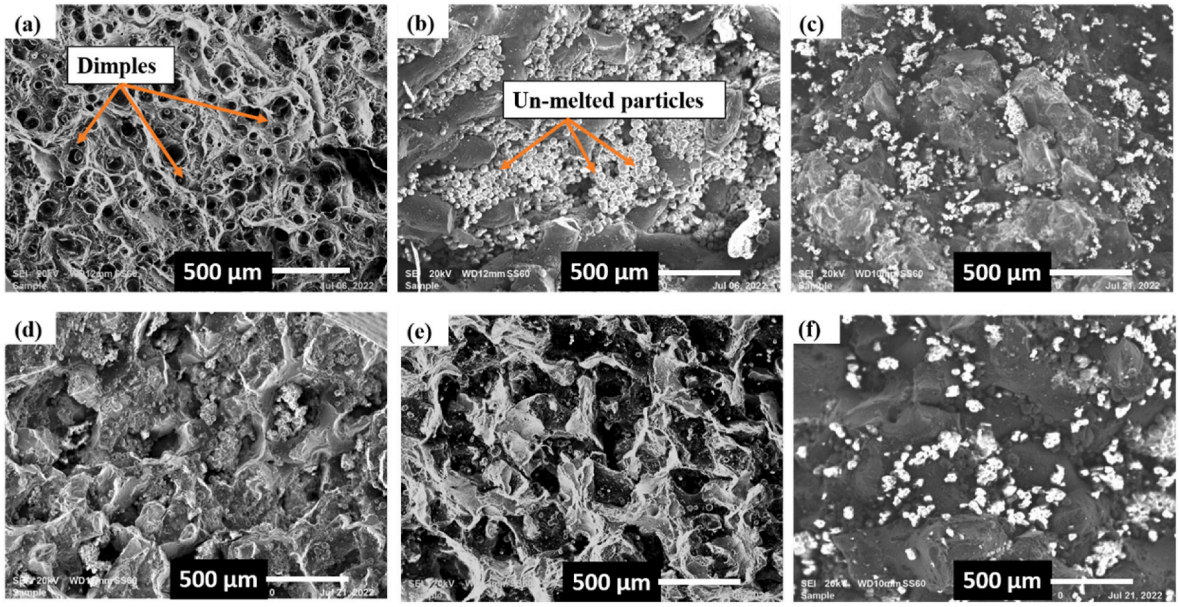

Fig. 5. SEM fracture morphology of the as-built AlSi12 as-built specimens at different laser power (W) and scanning speed (mm/s). (a) S2: 300 W-500 mm/s; (b) S3: 300 W-2500 mm/s; (c) S7: 175 W-1000 mm/s; (d) S11: 300 W-1500 mm/s; (e) S12: 175 W-500 mm/s; (f) S14: 250 W-1500 mm/s.

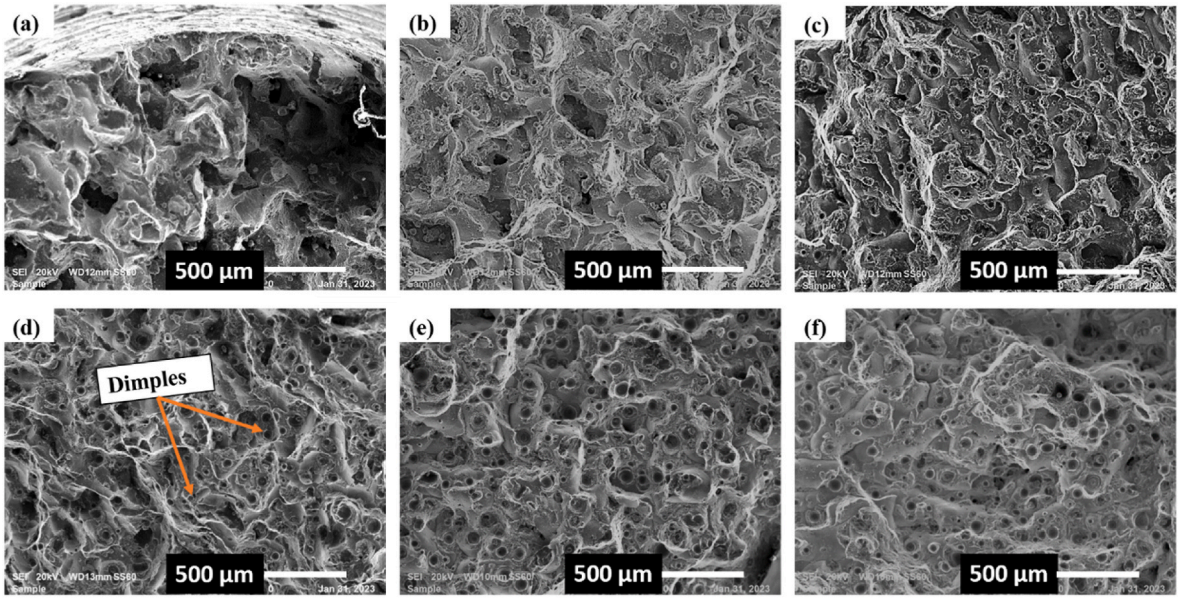

Fig. 6. SEM images of the fractured surface of batch 2 at different laser powers (W). (a) A: 175 W; (b) B: 200 W; (c) C; 225 W; (d) D: 250 W; (e) E: 275 W; (f) F: 300 W.

Table 6
ANOVA summary for the two-factor interaction model (2FI) for the relative density.

Source	Coefficient Estimation	Sum of squares	df	Mean square	F-value	p-value	
Model	81.97	126.35	3	42.12	1778.55	<0.0001	significant.
A-Laser Power	7.97	32.33	1	32.33	1365.35	<0.0001	
B-Scanning Speed	−11.27	72.29	1	72.29	3052.69	<0.0001	
AB	6.07	11.75	1	11.75	496.28	<0.0001	
Residual		0.2131	9	0.0237			
Cor Total		126.56	12				

*R^2 = 0.9983; A\djusted R^2 = 0.9978; Predicted R^2 = 0.9967; Adeq precision = 98.3023.

the mathematical model through the statistics coefficients R^2, Adjusted R^2, Predicted R^2, and Adequate (Adeq) precision. The Adeq precision is higher than 4 for all the models, which indicates an adequate signal, and the design space can be navigated by the models. Furthermore, the difference between the adjusted R^2 and the predicted R^2 is less than 0.2 for all models, implying the reliability of the collected data [13].

Table 7
ANOVA summary for the 2FI hardness response.

Source	Coefficient Estimation	Sum of squares	df	Mean square	F-value	p-value	
Model	31.57	7611.34	3	2537.11	139.96	<0.0001	significant.
A-Laser Power	74.1	2802.33	1	2802.33	154.59	<0.0001	
B-Scanning Speed	−99.70	5657.45	1	5657.45	312.08	<0.0001	
AB	72.17	1662.95	1	1662.95	91.73	<0.0001	
Residual		163.15	9	18.13			
Cor Total		7774.49	12				

*$R^2 = 0.9790$; Adjusted $R^2 = 0.9720$; Predicted $R^2 = 0.9593$; Adeq precision = 24.2239.

Table 8
Summary of ANOVA summary for 2FI UTS response.

Source	Coefficient Estimation	Sum of squares	df	Mean square	F-value	p-value	
Model	−89.07	1.903E+05	3	63444.15	408.30	<0.0001	significant.
A-Laser Power	249.07	31581.17	1	31581.17	203.24	<0.0001	
B-Scanning Speed	−342.13	66616.94	1	66616.94	428.72	<0.0001	
AB	83.71	2237.04	1	2237.04	14.40	0.0043	
Residual		1398.46	9	155.38			
Cor Total		1.917E+05	12				

*$R^2 = 0.9927$; Adjusted $R^2 = 0.9903$; Predicted $R^2 = 0.9858$; Adeq precision = 51.7829.

Table 9 shows the data of the optimisation process with the actual and predicted values of the responses studied. The comparative analysis of the results indicates that the experimental results correlate with the predictive model. This demonstrates a good correlation in the fitting of the RSM model with the experimental procedure.

Table 10 presents the mean and standard deviation of the predicted model. The predicted means and median can be identified in the coded Eqs. (5)–(7). Standard deviation and mean values indicate that there are no outliers in the residual versus run report. The results obtained from the experiments are within the range of the predicted values.

4.1. Evaluation of the proposed model by analysis of the effect of process parameters on the material properties

4.1.1. Relative density

The results shown in Fig. 7 (a) indicate the interaction of the factors with the relative density. It suggests that as the laser power increases, the relative density becomes higher. Although the increase in scan speed drastically reduced the relative density, as presented in Fig. 7(b) The predicted versus actual graph shows that the predictive model agrees with the experimental results. The points are very close to the fitted line. This means that Eq. (4) demonstrates that the CCD approach fits the experimental design. Fig. 7(c) shows that the effect of laser power is central to achieving a higher relative density [40]. The increase in scan speed caused thermal distortion and microstructural defects, which consequently affected the densification of the material. In the second density test, it was found that the relative density increased from 95.14 to 97.48 as the laser power increased from 175 W to 300 W (see Fig. 8). The porosity observed in the microstructure was also less (Fig. 4). The constant scan speed allowed the previous layer to be fully melted.

Table 9
Report on the predicted and actual values of the responses.

	S2	S3	S7	S11	S12	S14
Actual relative density (%)	95.14	87.44	87.73	90.08	93.19	86.51
Predicted Relative Density (%)	94.24	86.69	87.40	90.61	93.43	86.92
Actual hardness (HV)	133.3	76.2	77.9	101.8	132.6	82.7
Predicted Hardness (HV)	134.37	76.74	82.19	105.56	129.38	77.33
Actual UTS (MPa)	418.42	38.71	71.67	148.38	256.93	79.72
Predicted UTS (Mpa)	374.70	16.85	74.94	195.78	254.48	75.63

Previous studies have obtained a relative density of 95 % and 99 % with laser power varying from 180 W to 300 W and scan speed at 500 mm/s [8,40]. The characteristics of the powder were essential to determine the flowability during the process. Hence, it is worth noting that the variation in the results is due to different types of powder and laser spot sizes.

4.1.2. Hardness analysis

The hardness of Al–Si12 fabricated by SLM is an important element in determining the desirable industrial application, as the values are related to the resistance of Al–Si12 to wear from friction [15]. The highest values of hardness measured in the first batch are from S2 (133.3 HV) and S12 (132.6) with their respective laser power at 300 W and 175 W and the same scan speed of 500 mm/s. Fig. 9 highlights the different representations of the impact of the variants on the hardness. The predicted values are in line with the experimental results. The hardness of the specimens varied significantly with the change in laser power as presented in Fig. 10. During the SLM building process, the fine grains generated by the high cooling rate in the molten pool prevent the nuclei from developing coarsely in the microstructure. The coarser the microstructure, the softer the material becomes [42]. This correlates with the microstructure of the samples in the first and second batches. The samples with higher density achieved a hardness of 116 ± 17 HV. These values are higher compared to the AlSi12 parts produced by casting, which have a hardness value of 64±4 HV [41]. However, in the second batch the values of samples A (70.8 HV) and F (116.6 HV) with their equivalent in the first batch, as S2 (133.3 HV) and S12 (132.6 HV) differ drastically. This can be attributed to the indenter meeting a keyhole pore, agglomeration of silicon in the microstructure or poor overlapping of the melting pool [31]. Therefore, it implies that the hardness was not the same on all surfaces, which affected the average of the overall samples.

4.1.3. Analysis of the ultimate tensile strength

In Fig. 11, it is inherent in (a) that the scan speed has a significant effect, as well as the laser power on the UTS. Fig. 11 (b) shows that the actual points are evenly distributed on the sides of the line, which validates the accuracy of the predicted Eq. (7) generated by the design software. In Fig. 11 (c), the 3D plot shows the graph of the UTS model with the variants. The UTS reaches maximum at higher laser power. This can be ascribed to the resulting values of the process parameters in batch 1 and batch 2. The outstanding UTS (415 ± 3 MPa) in both cases are found at a laser power of 300 W and a scan speed of 500 mm/s. This

Table 10
Point of prediction.

Analysis	Predicted Mean	Predicted Median	Std Dev	SE Mean	95 % CI low for mean	95 % CI high for mean	95 % TI low for 99 % Pop	95 % TI high for 99 % Pop
Relative Density	81.96	81.96	0.15	0.16	81.59	82.34	81.001	82.93
Hardness	31.57	31.57	4.257	4.57	21.22	41.91	4.84	58.30
Ultimate tensile strength	−89.07	−89.07	12.46	13.38	−119.36	−58.78	−167.32	−10.82

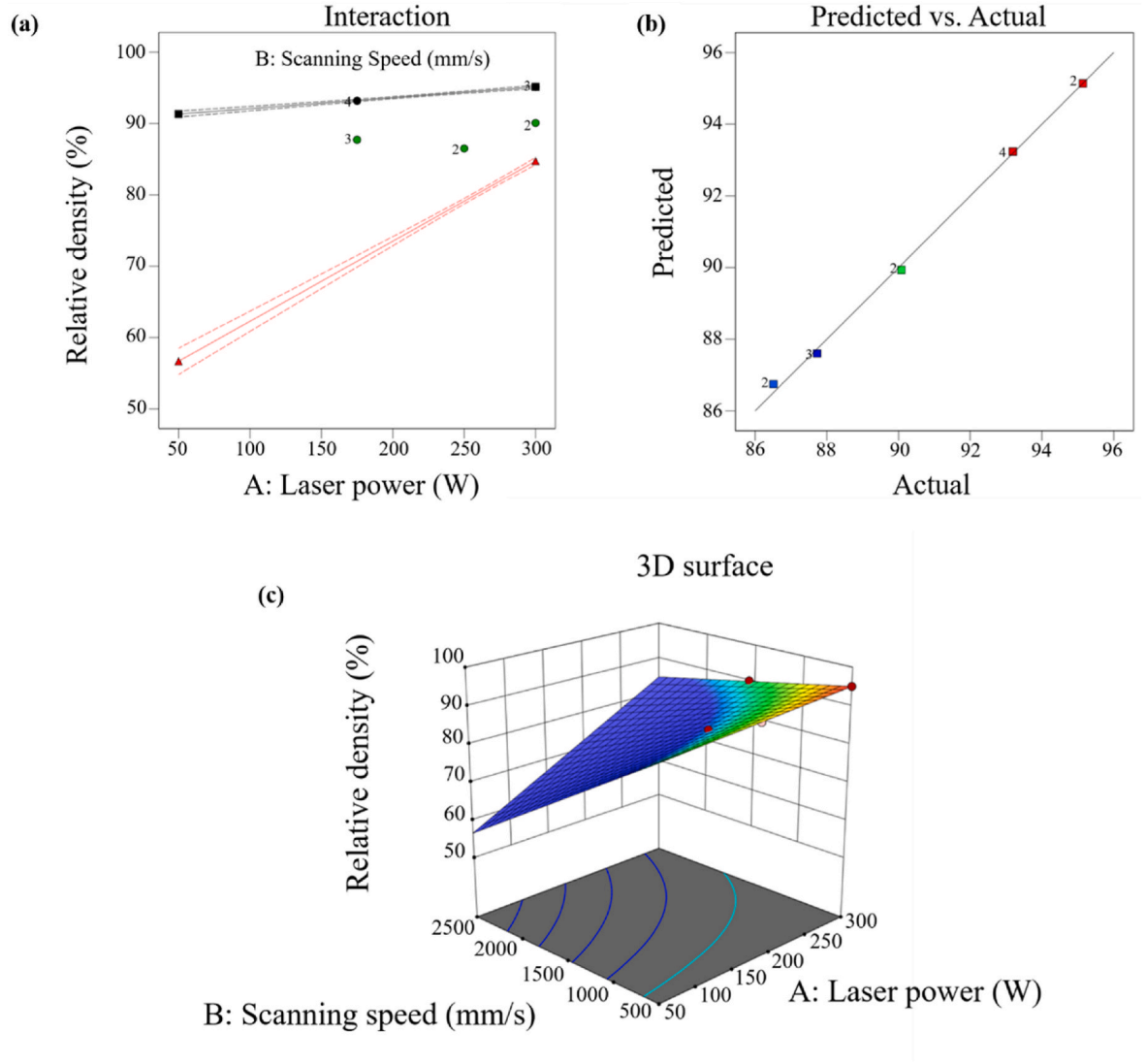

Fig. 7. Factorial graph interaction; (a) actual interaction; (b) predicted versus actual; (c) contour plot.

finding suggests that the densification of the samples has less of an impact on the strength of the material. The fracture morphology showed numerous dimples (S3, S7, S11, and S14), resulting in lower strength (38–148 MPa). The latter results are considered lower than the threshold of the cast AlSi12, which, is 192 MPa [8]. Furthermore, crack propagation could occur due to surface defects with increasing load. As a result of the adhesion of the unmelted powder particles to the surfaces, the samples (S3, S7, S11, and S14), are considered unfit for industrial applications.

The samples built in the second experiment from the results in Fig. 12 showed considerable UTS values, this correlates with the literature in Table 4. Taking into account the microstructure of the samples, the larger grain boundaries could have inhibited the movement of dislocation and consequently improved the strength of the material [42]. The importance of increased laser power is consistent with the other responses. Noting that hardness is related to the tensile behaviour of the material, this implies that low densification is a source of defects that lead to low UTS and hardness.

5. Conclusions

In this study, the processing window optimisation employs RSM to statistically determine the SLM combination of ideal process laser parameters. The physical and mechanical properties of the AlSi12 samples constructed were investigated after two sets of experiments. The findings of the study are as follows:

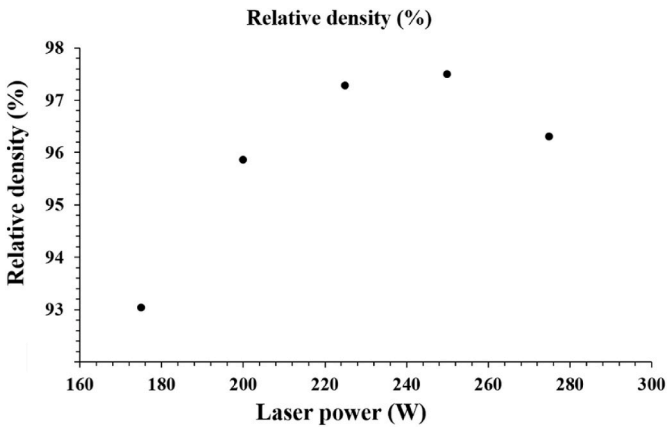

Fig. 8. Relative density from batch 2.

- A process window was narrowed after varying the laser power and the scan speed in the range of 50 W–300 W and 500 mm/s to 2500 mm/s. The higher level of scan speed (from 1500 mm/s to 2500 mm/s) resulted in a nonoptimal combination of process parameters with a lack of fusion defects.
- In the first experiment, the laser power of 200 W and the scanning speed of 500 mm/s were found to be a feasible combination. With a relative density of 95.14 %, a UTS of 418.42 MPa and a hardness of 133.3 HV. In the second experiment, the relative density increased to 97.4 %, while the hardness decreased to 118.6 HV and the UTS to 415.58 MPa.
- The observed changes in the grain boundaries of the microstructure, inhomogeneity, and porosity influenced the hardness and UTS in the two sets of experiments. The overlap of successive layers and the remelting of the previous impacted the distributions of the pores. This was attributed to the laser power intensity in the molten pool.
- The fracture analysis of some selected samples shows evidence of dimples (S2, S12, C, D, E, and F), intergranular cleavages (S 3 and 14), small dimples, and minimal crack propagation (S7 and 11) on the surface.

Parametric interaction highlighted that the sample produced with similar scan speed value of 500 mm/s (S2 S12, A, B, C, D, E and F) exhibited a higher UTS. The research findings also indicate that the lower value (500 mm/s) of the scan speed in this study was enough to fabricate fully consolidated samples with the laser power values ranging from 200 W to 300 W. Therefore, this study contributes to the existing knowledge, both in practice and in theory for the processing of AlSi12 via SLM. The developed predictive model equation can assist manufacturers using AM technology to produce AlSi12 parts in determining the general effects of laser scan speed and laser power on the physical and mechanical properties of the sample.

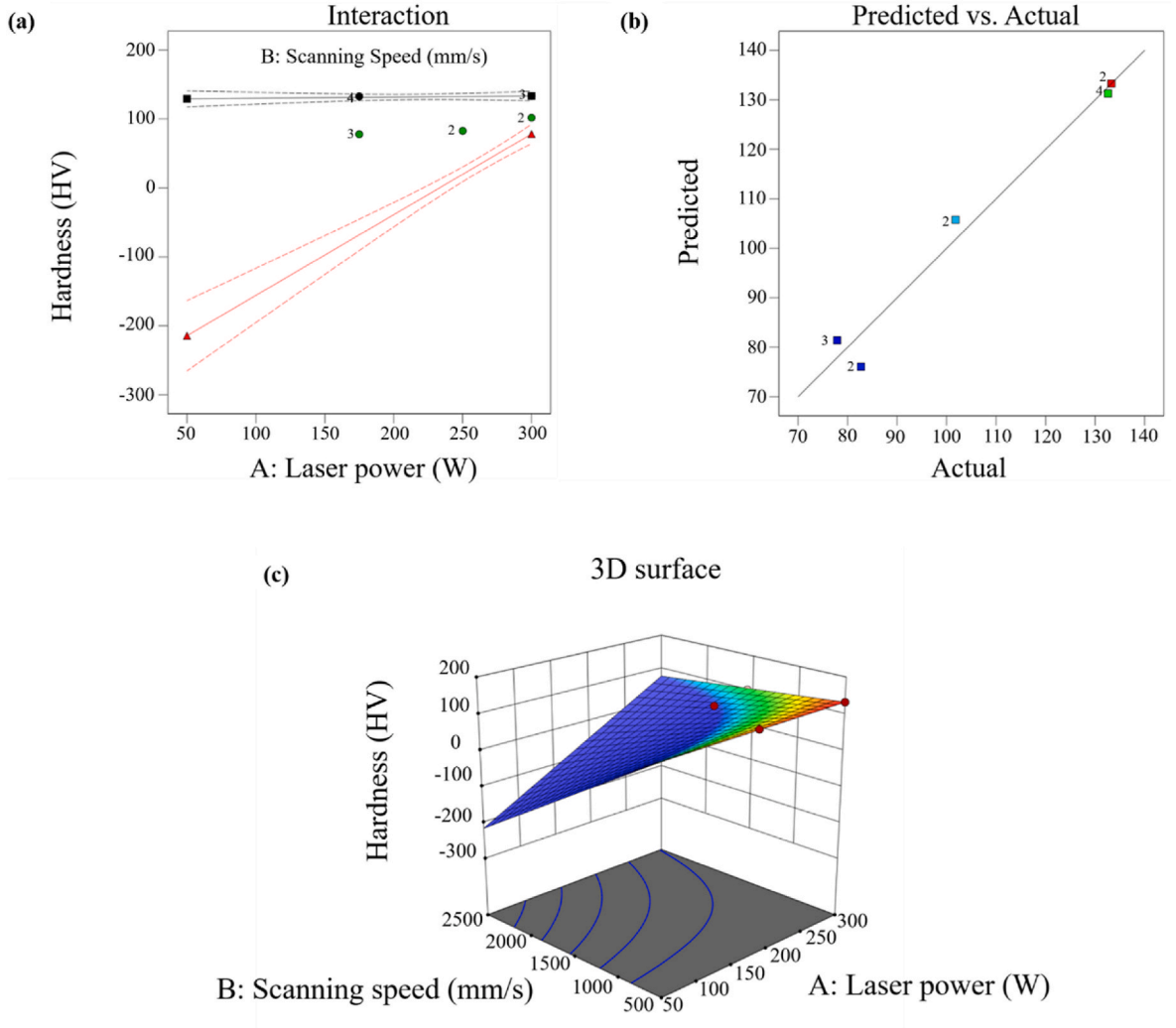

Fig. 9. Interaction of variants with hardness; (a) all factors; (b) predicted vs. actual plot; (c) contour plot.

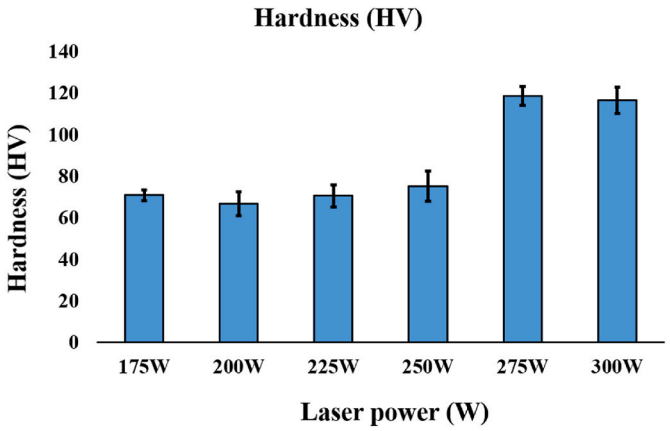

Fig. 10. Hardness values of AlSi12 for batch 2 samples.

Further studies will involve increasing the laser power while considering the focal diameter, varying the hatch spacing and layer thickness to decrease defects such as porosity that affect the density, microstructure, and mechanical properties of the material.

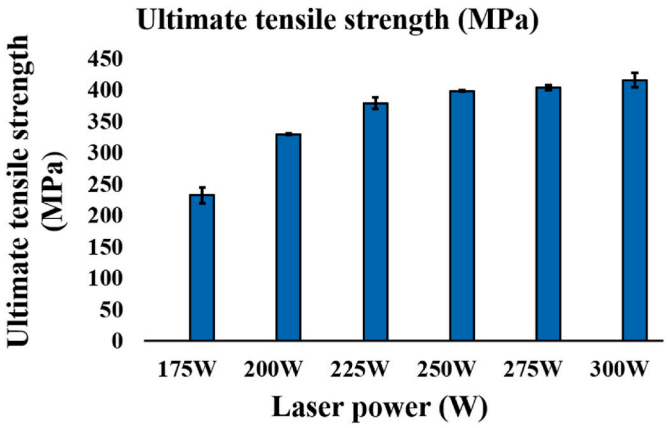

Fig. 12. Ultimate tensile strength results from batch 2.

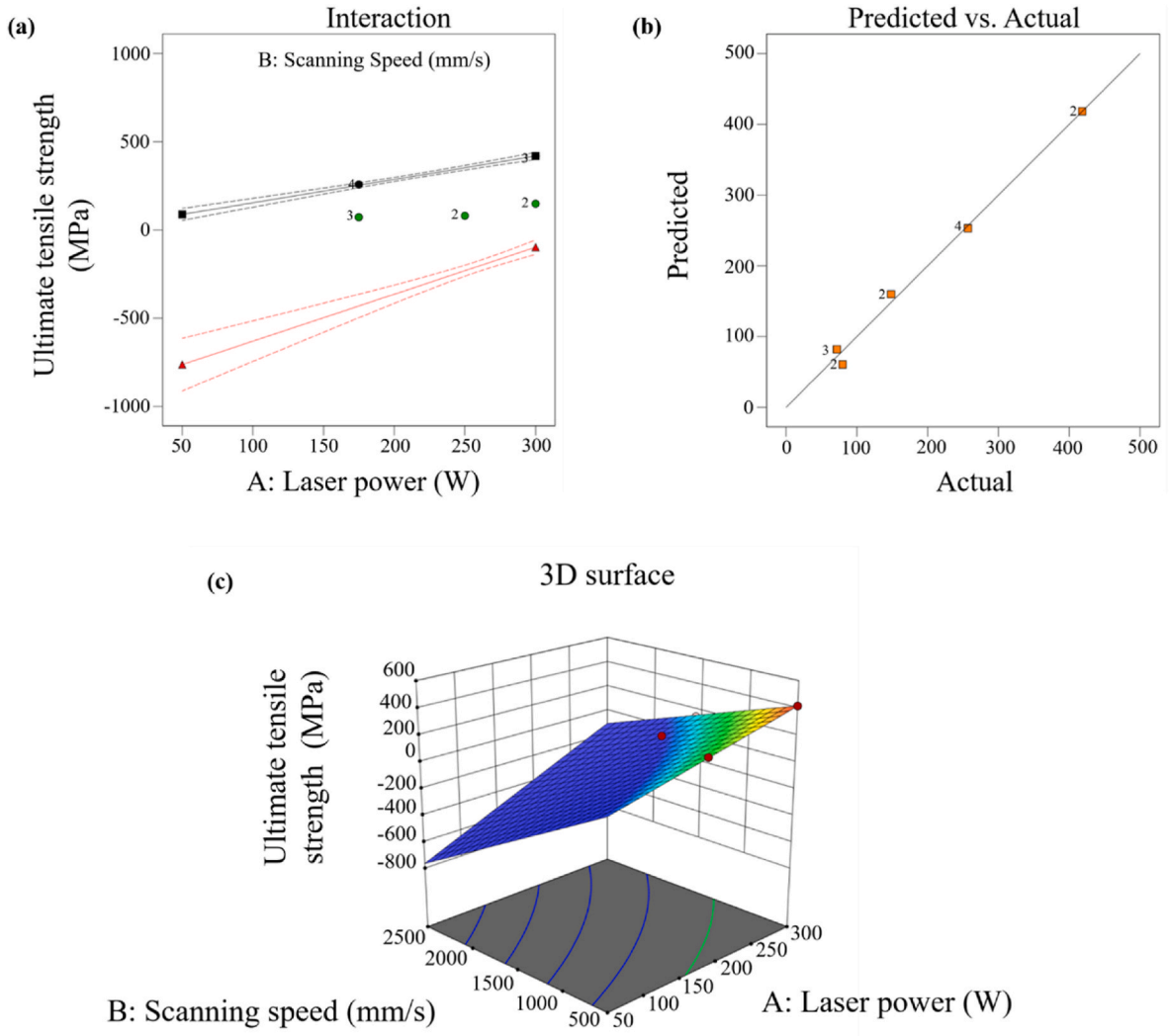

Fig. 11. Interaction of factors for UTS; (a) All factors; (b) Predicted vs. actual; (c) Contour plot.

Author contributions

It is a collaborative effort of all authors.

Funding

The National Research Foundation, grant number 144789, funded this research.

Declaration of competing interest

The authors declare that they have no known competing financial interests or personal relationships that could have appeared to influence the work reported in this paper.

Acknowledgements

The authors would like to thank Metal Heart for the production of the samples and Mr. Stephen Masete for his assistance in conducting the tensile tests. They also acknowledge the support and assistance of the Department of Industrial Engineering at Tshwane University of Technology, the Council for Scientific and Industrial Research (CSIR), and the Collaborative Programme on Additive Manufacturing (CPAM).

References

[1] Zhang J, Song B, Wei Q, Bourell D, Shi Y. A review of selective laser melting of aluminium alloys: processing, microstructure, property and developing trends. J Mater Sci Technol 2019;35(2):270–84.
[2] Wang Z, Ummethala R, Singh N, Tang S, Suryanarayana C, Eckert J, Prashanth KG. Selective laser melting of aluminum and its alloys. Materials 2020;13(20):4564.
[3] Olakanmi EO, Cochrane R, Dalgarno K. A review on selective laser sintering/melting (SLS/SLM) of aluminium alloy powders: processing, microstructure, and properties. Prog Mater Sci 2015;74:401–77.
[4] Aboulkhair NT, Simonelli M, Parry L, Ashcroft I, Tuck C, Hague R. 3D printing of Aluminium alloys: additive Manufacturing of Aluminium alloys using selective laser melting. Prog Mater Sci 2019;106:100578.
[5] Kotadia HR, Gibbons G, Das A, Howes PD. A review of laser powder bed fusion additive manufacturing of aluminium alloys: microstructure and properties. Addit Manuf 2021;46:102155.
[6] Aboulkhair NT, Everitt NM, Ashcroft I, Tuck C. Reducing porosity in AlSi10Mg parts processed by selective laser melting. Addit Manuf 2014;1–4:77–86.
[7] Aboulkhair NT, Maskery I, Tuck C, Ashcroft I, Everitt NM. The microstructure and mechanical properties of selectively laser melted AlSi10Mg: the effect of a conventional T6-like heat treatment. Mater Sci Eng: A 2016;667:139–46.
[8] Kang N, Coddet P, Dembinski L, Liao H, Coddet C. Microstructure and strength analysis of eutectic Al-Si alloy in-situ manufactured using selective laser melting from elemental powder mixture. J Alloys Compd 2017;691:316–22.
[9] Prashanth K, Scudino S, Eckert J. Defining the tensile properties of Al-12Si parts produced by selective laser melting. Acta Mater 2017;126:25–35.
[10] Fefelov AS, Merkushev AG, Chikova OA. Microstructure and mechanical properties of Al-12Si produced by selective laser melting. IOP Conf Ser Earth Environ Sci 2017;87:092011.
[11] Bai Y, Yang Y, Xiao Z, Zhang M, Wang D. Process optimization and mechanical property evolution of AlSiMg0.75 by selective laser melting. Mater Des 2018;140:257–66.
[12] Gokuldoss Prashanth K, Scudino S, Eckert J. Tensile properties of Al-12Si fabricated via selective laser melting (SLM) at different temperatures. Technologies 2016;4(4):38.
[13] Shim D-s. Effects of process parameters on additive manufacturing of aluminium porous materials and their optimization using response surface method. J Mater Res Technol 2021;15:119–34.
[14] Singh S, Sharma VS, Sachdeva A, Sinha SK. Optimization and analysis of mechanical properties for selective laser sintered polyamide parts. Mater Manuf Process 2013;28(2):163–72.
[15] Nandhakumar R, Venkatesan K. A process parameters review on Selective laser melting-based additive manufacturing of Single and Multi-Material: microstructure, Properties, and machinability aspects. Mater Today Commun 2023:105538.
[16] Buchbinder D, Schleifenbaum H, Heidrich S, Meiners W, Bültmann J. High power selective laser melting (HP SLM) of aluminum parts. Phys Procedia 2011;12:271–8.
[17] Zhuo L, Wang Z, Zhang H, Yin E, Wang Y, Xu T, Li C. Effect of post-process heat treatment on microstructure and properties of selective laser melted AlSi10Mg alloy. Mater Lett 2019;234:196–200.
[18] Mathe NR, Tshabalala LC. The validation of the microstructural evolution of selective laser-melted AlSi10Mg on the in-house built machine: energy density studies. Prog Addit Manuf 2019;4:431–42.
[19] Limbasiya N, Jain A, Soni H, Wankhede V, Krolczyk G, Sahlot P. A comprehensive review on the effect of process parameters and post-process treatments on microstructure and mechanical properties of selective laser melting of AlSi10Mg. J Mater Res Technol 2022;21:1141–76.
[20] Prashanth KG, Scudino S, Maity T, Das J, Eckert J. Is the energy density a reliable parameter for materials synthesis by selective laser melting? Mater Res Lett 2017;5(6):386–90.
[21] Scipioni Bertoli U, Wolfer AJ, Matthews MJ, Delplanque J-PR, Schoenung JM. On the limitations of volumetric energy density as a design parameter for selective laser melting. Mater Des 2017;113:331–40.
[22] Mathe NR. Development of ideal processing parameters for powder bed fusion system processing of AlSi10Mg using design of experiments. Journal of physics: conference series. IOP Publishing; 2021, 012019.
[23] Terner M, Ricordel T, Cho J-H, Lee J-S. The response surface methodology for optimizing the process parameters of selective laser melting. J Weld Join 2019;37(1):27–39.
[24] Chelladurai SJS, Murugan K, Ray AP, Upadhyaya M, Narasimharaj V, Gnanasekaran S. Optimization of process parameters using response surface methodology: a review. Mater Today Proc 2021;37:1301–4.
[25] Fatemi SA, Ashany JZ, Aghchai AJ, Abolghasemi A. Experimental investigation of process parameters on layer thickness and density in direct metal laser sintering: a response surface methodology approach. Virtual Phys Prototyp 2017;12(2):133–40.
[26] Solution S. Production-ready selective laser melting 280. https://www.slm-solutions.com/fileadmin/Content/Case_Studies/Production-Ready-Selective-Laser-Melting-SLM280-2.0.pdf.
[27] Breig SJM, Luti KJK. Response surface methodology: a review on its applications and challenges in microbial cultures. Mater Today Proc 2021;42:2277–84.
[28] Nzengue AGB, Mpofu K, Mathe N, Daniyan I, Muvunzi R. An experimental investigation of selective laser process parameters on aluminium alloy (AlSi12). Procedia CIRP 2023;118:638–42. 29.
[29] Chelladurai SJS, K M, Ray AP, Upadhyaya M, Narasimharaj V, S G. Optimization of process parameters using response surface methodology: a review. Mater Today Proc 2021;37:1301–4.
[30] Collins P, Brice D, Samimi P, Ghamarian I, Fraser H. Microstructural control of additively manufactured metallic materials. Annu Rev Mater Res 2016;46:63–91.
[31] Zhao L, Song L, Macías JGS, Zhu Y, Huang M, Simar A, Li Z. Review on the correlation between microstructure and mechanical performance for laser powder bed fusion AlSi10Mg. Addit Manuf 2022;56:102914.
[32] Li XP, Wang XJ, Saunders M, Suvorova A, Zhang LC, Liu YJ, Fang MH, Huang ZH, Sercombe TB. A selective laser melting and solution heat treatment refined Al–12Si alloy with a controllable ultrafine eutectic microstructure and 25% tensile ductility. Acta Mater 2015;95:74–82.
[33] Rashid R, Masood SH, Ruan D, Palanisamy S, Rahman Rashid RA, Elambasseril J, Brandt M. Effect of energy per layer on the anisotropy of selective laser melted AlSi12 aluminium alloy. Addit Manuf 2018;22:426–39.
[34] Wang XJ, Zhang LC, Fang MH, Sercombe TB. The effect of atmosphere on the structure and properties of a selective laser melted Al–12Si alloy. Mater Sci Eng: A 2014;597:370–5.
[35] Pastirčák R, Brůna M, Bolibruchová D. The influence of different wall thicknesses of the casting in the direct squeeze casting. Arch Foundry Eng 2019;19(1).
[36] Ponnusamy P, Masood SH, Ruan D, Palanisamy S, Rashid R. High strain rate dynamic behaviour of AlSi12 alloy processed by selective laser melting. Int J Adv Des Manuf Technol 2018;97(1):1023–35.
[37] Rathod HJ, Nagaraju T, Prashanth K, Ramamurty U. Tribological properties of selective laser melted Al12Si alloy. Tribol Int 2019;137:94–101.
[38] Suryawanshi J, Prashanth KG, Scudino S, Eckert J, Prakash O, Ramamurty U. Simultaneous enhancements of strength and toughness in an Al-12Si alloy synthesized using selective laser melting. Acta Mater 2016;115:285–94.
[39] Siddique S, Imran M, Rauer M, Kaloudis M, Wycisk E, Emmelmann C, Walther F. Computed tomography for characterization of fatigue performance of selective laser melted parts. Mater Des 2015;83:661–9.
[40] Baitimerov R, Lykov P, Zherebtsov D, Radionova L, Shultc A, Prashanth KG. Influence of powder characteristics on processability of AlSi12 alloy fabricated by selective laser melting. Materials 2018;11(5):742.
[41] Chou R, Milligan J, Paliwal M, Brochu M. Additive manufacturing of Al-12Si alloy via pulsed selective laser melting. J Occup Med 2015;67(3):590–6.
[42] Suryawanshi, J.; Prashanth, K.; Scudino, S.; Eckert, J.; Prakash, O.; Ramamurty, U., Simultaneous enhancements of strength and toughness in an Al-12Si alloy synthesized using sele.